Macro and Micro Analysis on Coal-bearing Soil Slopes Instability Based on CFD-DEM Coupling Method

Hong Zhang (hongzhang@nit.edu.cn)
School of Civil and Architectural Engineering, Nanchang Institute of Technology
Bang Zhang
School of Civil and Architectural Engineering, Nanchang Institute of Technology
Haoran Feng
School of Civil and Architectural Engineering, Nanchang Institute of Technology
Can Wu
School of Civil and Architectural Engineering, Nanchang Institute of Technology
Kun Chen
School of Civil and Architectural Engineering, Nanchang Institute of Technology

Research Article

Keywords: discrete element method (DEM), computational fluid dynamics (CFD), microscopic computational model , coal-bearing, rainfall

Posted Date: February 3rd, 2021

DOI: https://doi.org/10.21203/rs.3.rs-154715/v1

Macro and Micro Analysis on Coal-bearing Soil Slopes Instability Based on CFD-DEM Coupling Method

Hong Zhang，Bang Zhang，Haoran Feng, Can Wu, & Kun Chen

School of Civil and Architectural Engineering, Nanchang Institute of Technology, Nanchang 330099, China

Correspondence should be addressed to Hong Zhang；hongzhang@nit.edu.cn

Abstract: By combining the discrete element method (DEM) with computational fluid dynamics (CFD), a three-dimensional CFD–DEM fluid–solid coupling microscopic computational model was established to analyse the micro-mechanism of instability and failure in a coal-bearing soil slope during rainfall. According to the results, the main failure mode of coal-bearing soil slopes simulated by the CFD–DEM fluid–solid coupling model was rainwater washing, and the slope sliding surface was predicted as an approximately linear segment. The adaptability of this numerical method was verified by considering its similarity to a range of rain-washed slopes in an outdoor model test. During rainfall, microscopic parameters, such as force chain and coordination number slope soil particles, changed, as confirmed by changes in the coordination number of the slope's top particles from 6.0 in the initial state to 3.2 in the unstable state. This was directly related to the macroscopic mechanics of the slope soil. In this study, based on the analysis of the changes in the microscopic parameters of the particles, the law of failure evolution of coal-bearing soil slopes during rainfall was explored from the microscopic perspective. This study not only provides a theoretical basis for the protection design and construction of coal-bearing soil slopes in the region but also encourages an effective analytical method for the macroscopic mechanical law of discrete media from a micro-macro perspective in geotechnical engineering.

Introduction

In the case of rainfall, rainwater will infiltrate into the soil pores of the slope. When the pores of soil are completely filled with rainwater, saturated soil will be formed. Hence, the shear strength and stability of slope soil will be reduced under the infiltration of rainwater. Traditional continuous coupling models of saturated soils are usually based on homogenising mixture theories, such as Biot's theory or micromechanical equations of motion[1,2]. This requires some form of a constitutive relation to describe the stress–strain relation of the solid phases. Among such constitutive relations, the hat model, multiple-yield surface plasticity model and bounding surface plasticity model are the most representative models. The aforementioned continuous mechanical models for saturated soil simulation are based on the phenomenological description of solid–liquid binary phases. Several assumptions exist in the field of equation and constitutive relations. For example, in general, the initial local porosity equals the overall average porosity, the momentum exchange between phases follows Darcy's law and the permeability coefficient is independent of strain. Nevertheless, Darcy's law is essentially a low-order Navier–Stokes equation, which is functional only when the pore flow is laminar and the inertial forces are negligible [3]. High hydraulic gradients can cause non-laminar motion, and changes in porosity due to the increased volumetric deformation of soil skeleton can also lead to deviations from Darcy's law[4] .Therefore, establishing a fluid–solid coupling micro-mechanical model for slopes from the micro–macro perspective is necessary. The model considers the effects of rain to demonstrate discrete skeleton deformation, pore fluid flow and mutual coupling due to multi-scale and multi-phase couplings.

In the Euler-Lagrange method, rock and soil masses are generally considered to have discrete particles with specific spatial sizes and shapes, dividing a continuous fluid into several grid units. The average

characteristics of fluid in a grid unit are considered representative of the characteristics of the entire unit. This avoids the low computational efficiency caused by the calculation of microscopic pore-water movement characteristics between soil particles. In such methods, discrete element method (DEM) is usually used for discrete media calculations and computational fluid dynamics (CFD) is used for fluid calculations. In the early days, CFD–DEM fluid–solid coupling methods were mostly applied in the industrial field. For example, Tsuji et al. [5] performed the coupling of CFD and DEM to simulate the behaviour of gas flow in solid particles. In the dynamic collision model proposed by Xu and Yu [6], the same temporal and spatial scales were set for CFD and DEM and Newton's third law was used to describe fluid–particle interactions. Subsequently, Xu et al. [7] and Yu and Xu [8] further improved the basis for simulating the movements between solid and fluid phases. Other scholars also used CFD–DEM coupling method to carry out relevant research[9-19].

The CFD–DEM fluid–solid coupled model was applied in the field of geotechnical engineering with some delay. Shamy and Zeghal[20] applied this method in geotechnical analyses. The Navier–Stokes equation was simplified and a three-dimensional (3D) CFD–DEM coupling method was adopted to analyse seepage in slope soil. Simulation results showed that this method was effective in reflecting the micro-mechanism of seepage in slope soil. Following a similar research approach, several scientists applied the CFD–DEM coupling method in soil seepage and liquefaction studies and obtained favourable results[21-24]. Recently, through advanced developments based on commercial software PDF^{2D}, Jiang and Zhang [25] and Khalili and Mahboubi [26] embedded discrete CFD–DEM control equations in PDF^{2D}. They performed numerical simulations of single-particle free settling in water, one-sided drainage one-bit consolidation test and biaxial undrained compression test; they obtained ideal results. Wang et al. [27] adopted the particle rolling resistance model to simulate the effects of soil particle shape and introduced a model into the CFD–DEM coupling control equation. The results showed that the interparticle rolling resistance model introduced in the coupling model well documented the effects of particle shape on the angle of repose of sand piles and the porosity of soil deposits. The above studies suggested that application of CFD–DEM coupling model as a numerical simulation method is promising, especially for the micro–macro analysis of mutual coupling between soil and fluid.

In this study, a coal-bearing soil slope from the Wanzai-Yichun Expressway Project in Jiangxi Province was selected as the research target. Based on the CFD–DEM coupling methods, a 3D CFD–DEM fluid–solid micro-action calculation model was established for the soil slope. The failure mechanism of coal-bearing soil slope under rainfall was analysed, and the calculation results showed good agreement with the model test results. Therefore, the research results are expected to provide a theoretical basis for the protection design and construction of coal-bearing soil slopes in this region.

Methods

CFD-DEM coupling calculation process. Based on the business software PFC^{3D} of discrete element method, the program is written in fish language, which makes the data exchange between PFC^{3D} and its embedded CFD solver, so as to realize the coupling calculation of fluid and solid. The specific calculation process is as follows: firstly, the fluid control equations in the CFD module are discretized by the finite volume method according to the boundary conditions, and the discrete equations are solved by the PISO（Pressure Implicit Splitting of Operators）stress velocity coupling algorithm[28]. At the same time, the grid data is sent to the DEM module, through which the porosity and drag force are calculated, and then the data is sent back to the CFD module. Next, the force between the fluid and the particles in each time step control unit is sent to the DEM calculation module, and then the fluid force is applied to the soil particles by the discrete element method, and the mechanical calculation between the particles is carried out at the same time. Finally, the fluid forces and porosity are transferred back to the CFD model, so that the cycle calculation is completed until the end of the program.

Verification of fluid solid coupling program of CFD-DEM. Stokes law shows that the settlement velocity of a small ball under the action of gravity in water is certain, which is also the fundamental principle of measuring the gradation of fine-grained soil by densitometer method in geotechnical test. In this section, the fluid and solid coupling program proposed above is used to simulate the free falling motion of a single particle under the action of gravity in water, so as to verify the feasibility of the method.

The particles fall freely in the liquid, and their velocity tends to be stable after a certain time. In the fluid, solid particles will be affected by gravity, buoyancy and drag force. The motion equation of falling spherical particles is expressed as follows[29]:

$$\frac{4}{3}\pi r^3 \rho_p \frac{\mathrm{d}\vec{u}_z}{\mathrm{d}t} = \frac{4}{3}\pi r^3 (\rho_p - \rho_f)\ \vec{g} - \frac{1}{2}\pi r^2 \rho_f C_d \vec{u}_z^2 \tag{1}$$

where ρ_p is the density of the particle; ρ_f is the density of the fluid; r is the radius of the particle; $\vec{u}_z$ is the vertical velocity of the falling particle; and C_d is the drag coefficient.

As the settling velocity of particles tends to a constant value, the value of $\frac{\mathrm{d}\vec{u}_z}{\mathrm{d}t}$ is 0, and equation (1) can be simplified as follows:

$$\frac{4}{3}\pi r^3 (\rho_p - \rho_f)\ \vec{g} = \frac{1}{2}\pi r^2 \rho_f C_d \vec{u}_z^2 \tag{2}$$

When the Reynolds number R_{ep} is very small, the drag coefficient C_d can be simplified as follows:

$$C_d = \frac{24}{R_{ep}} \tag{3}$$

Therefore, the vertical velocity of the falling particle $\vec{u}_z$ can be solved by Stokes law, and it is expressed as follows:

$$\vec{u}_z = \frac{2}{9}\frac{r^2(\rho_p - \rho_f)\ \vec{g}}{\mu_f} \tag{4}$$

The two particles with a particle size of 1.5 mm and 2.0 mm are free to sink under the action of gravity in the fluid with static viscosity of 1 $\mathrm{Pa \cdot s}$, in which the particle density is 2400 kg / m^3 and the fluid density is 1000 kg / m^3. By substituting the above parameters into equation (4), the theoretical values of the final settling velocity of particles can be directly calculated, which are - 6.86 mm / s and - 12.1 mm / s, respectively.

After opening the CFD-DEM coupling program module in PFC software platform, the same fluid parameters are given after importing grid data. Particles of the same size and mass are generated in the fluid at the same time, and then sink freely under the action of gravity, and the final particle velocity tends to be stable. Finally, the simulation results for the velocity of 1.5 mm and 2 mm are - 6.89 mm / s and - 12 mm / s respectively, which are close to the theoretical results, as shown in Figure 1. It shows that the fluid particle interaction can be realized by the fluid solid coupling program in this paper.

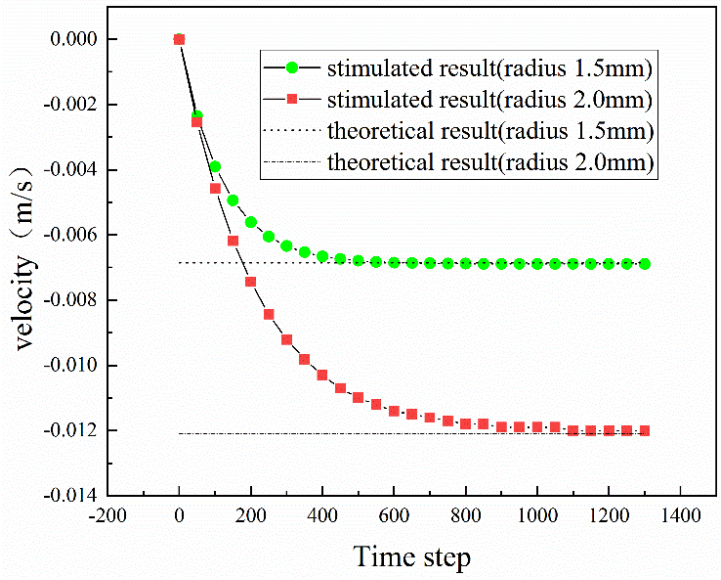

Figure 1. Velocity of falling particles.

Outdoor Test Model of Coal-bearing Soil Slope. To identify the failure mechanism of coal-bearing soil slopes during rainfall infiltration, the project team conducted outdoor slope model tests with artificial rainfall. A slope model box with a size of 4.5 × 3.0 × 2.4 m^3 (length × width × height) was designed. The test soil samples were taken from remolded soil exposed from the excavations on a coal-bearing soil slope at K30 + 120 in section A5 of the Wanzai-Yichun Expressway Project in Jiangxi Province. The slope model was filled with a layer of soil every 40 cm at a slope ratio of 1:1.5. The simulated rainfall intensity was set to 9.84 × 10^{-7} m/s, which corresponded to the average value of the maximum rainfall intensity in July and August in Yichun, Jiangxi Province in recent 10 years. The tests were conducted on November 19, 2018 from 8:00 am to 6:00 pm. Field observations (Fig. 2a) showed that water and soil loss as well as rainwater erosion were the main failure modes of slope stability, and resulted in the occurrence of erosion ditches of different depths, with a maximum depth of 0.36 m.

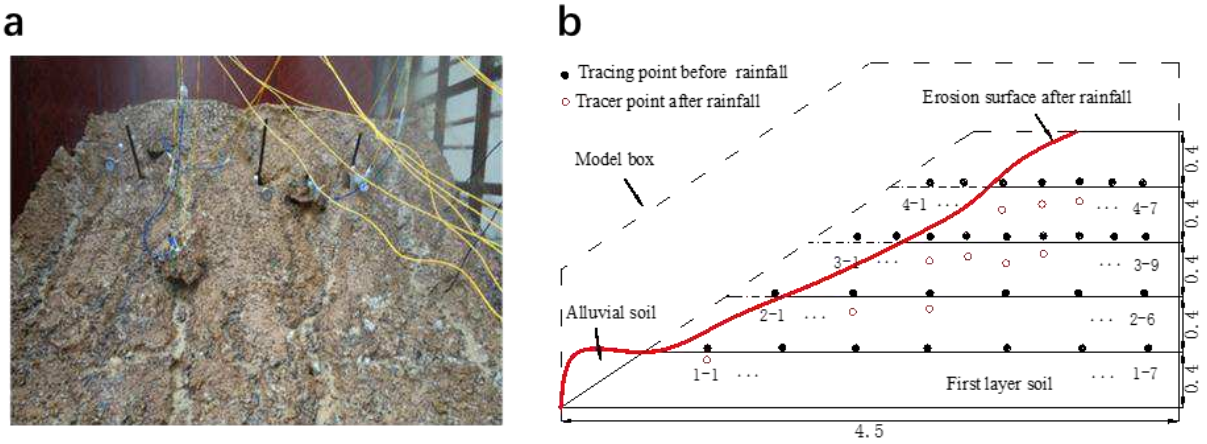

Figure 2. The site of slope failure test. **(a)** Front of slope model; **(b)** Schematic diagram of soil movement of tracer point on the site of slope failure test. (unit: m)

In the test, a total of 29 side tracer points in four rows were buried in the slope soil (Fig. 2b), and their movements were clearly visible through the Plexiglas side of the model box. The measurement results showed that during continuous rainfall, rain-wash, as the main failure mode of soil, formed erosion ditches at different depths from the slope surface. The ditches reached a maximum depth of 0.36 m in the mid-upper slope.

Numerical Calculation Model for Coal-bearing Soil Slope. As shown in Figure 3, a 3D microscopic computational model was established using the fish programming language for fluid–solid coupling (CFD–DEM) in a slope using an artificial rainfall model test. The simulation scenario was a model slope after artificial rainfall of 8 h. According to the field test results, the rainwater formed a transient saturated zone in the soil mass of the model slope with a penetration depth of about 0.5 m. To facilitate modelling and calculation, a straight line was used instead of a curve to represent the boundary between saturated and unsaturated soils. Figure 3(b) shows the soil seepage area. As shown in Figure 3(b), the fluid grid was extended along the front surface of the slope to match the real situation, as the particles moved down the slope due to surface runoff after rainfall.

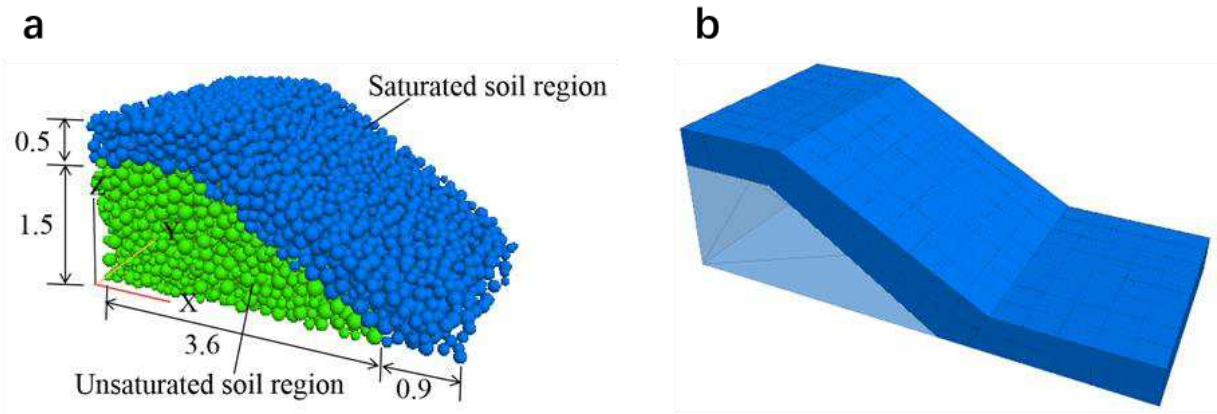

Figure 3. The fluid-solid coupling（CFD-DEM） calculation model of slope under rainfall infiltration. (**a)** The soil in the rainwater infiltration area is stratified;(**b)** Set up the seepage grid. (unit: m)

Figure 3(a) shows the 3D fluid–solid coupling calculation model of the slope under the influence of rainwater. As suggested by particle grouping, the particles in the model were divided into two groups. The blue particles in the upper part were in the rainwater saturated zone, comprising 2,646 particles, and the light green particles in the lower part were in the unsaturated zone of the slope, comprising 4,572 particles. In the unsaturated zone, the microscopic parameters of particles are determined according to the triaxial test results of numerical simulation, as shown in Table 1. Since the soil strength in the saturated zone was lower than that in the unsaturated zone, the bond strength of the soil in the saturated zone was reduced and the other parameters remained unchanged.

Friction μ	partical size （m）	k_n^{cb} （N/m）	k_s^{cb} （N/m）	e	dump	density （kg/m^3）	E_{mod} （P_a）	k_{ratio}
0.5	0.05~0.09	4.5×10^4	4.5×10^4	0.35	0.7	2400	3×10^6	2

Table 1. Microscopic parameters of coal bearing soil.

Based on the fluid characteristics and rainfall intensity of the model slope artificial rainfall, the fluid parameters acting on the saturated zone of the slope were set according to Table 2. The ratio of the Z-axis flow rate to the X-axis flow rate was set to 1:1.5 to ensure consistency between the fluid direction and the actual flow, while excluding the effect of the fluid on the Y-axis. As shown in Figure 4, the fluid flow direction was consistent with the slope runoff in the outdoor rainfall test.

density（kg/m^{-3}）	coefficient of viscosity（pa·s）	X-flow velocity（m/s）	Z-flow velocity（m/s）	Y-flow velocity（m/s）	mesh quantity
1000	0.001	0.33	-0.22	0	232

Table 2. Setting of fluid parameters in saturated soil.

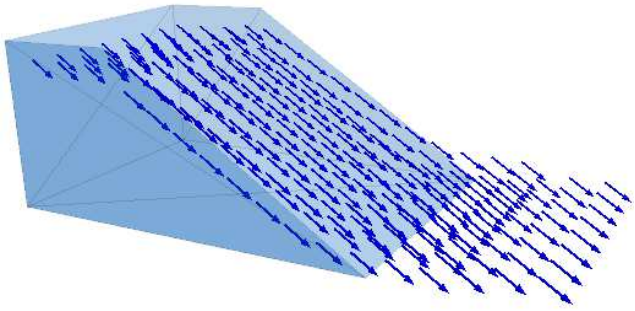

Figure 4. Direction of fluid movement in slope saturated area.

Calculation Results

Calculation results of soil particle trajectory on slope. Figure 5 shows the movement of soil particles on the side of the model after the simulation test. According to Figure 5(a), the particle displacement mainly occurred in the saturated zone, whereas it occurred only locally in the unsaturated zone. As shown in Figure 5(b), the particle displacement pattern shows that there was a sliding zone on the slope, which was drawn based on the middle section of the slope model using the CAD software. The displacement of the upper soil mass was about 0.9 m and that of the lower soil mass was about 1.7 m, with the simultaneous formation of an approximate linear sliding surface. Particles on the top of the slope were eroded with erosion depths of 0.3～0.4 m. This was in good agreement with the test results of the outdoor slope model.

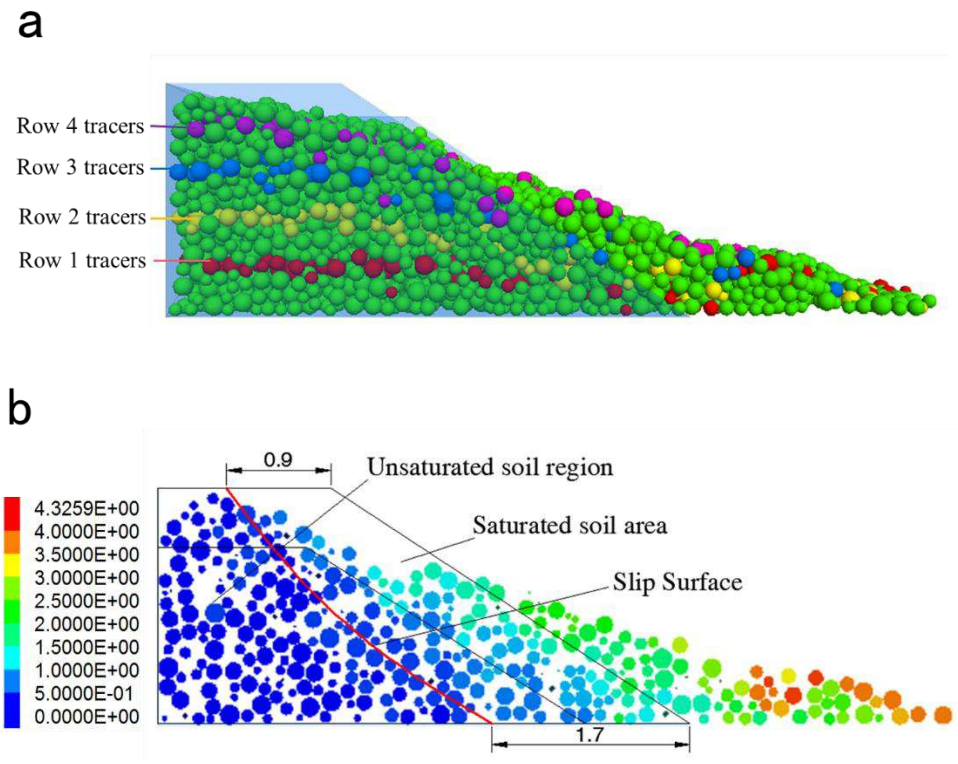

Figure 5. Schematic diagram of the overall particle movement of the slope. (**a**) Overall particle displacement diagram of slope;(**b**) Schematic diagram of slope sliding surface. (unit: m)

Calculation results of force chain of slope soil particles. Figure 6 shows the force chain evolution of the slope model during rainfall. In this figure, continuous rainfall makes the force chain sparse in the saturated zone of the slope, which shows small contact forces and instability between particles in that zone. When the fluid flowed in the upper slope, the force chain in the lower part of the unsaturated soil became dense and thick, suggesting a strong contact force between particles in the slope and soil stability in that zone. In addition, the force chain stretched significantly along the slope. As the slope became gentle, the force chain at the top of the slope decreased and became sparse, implying a significant particle displacement in the saturated zone. As shown in Figure 6(d), at the 100,000 time step, the force chain of soil particles in the unsaturated zone remained basically unchanged. In contrast, the particles on the slope surface of the saturated zone decreased and became sparse. This indicates that particles on the slope surface continued to move downward and accumulated at the foot of the slope, explaining the thick and dense force chains at the foot of the slope and on the ground.

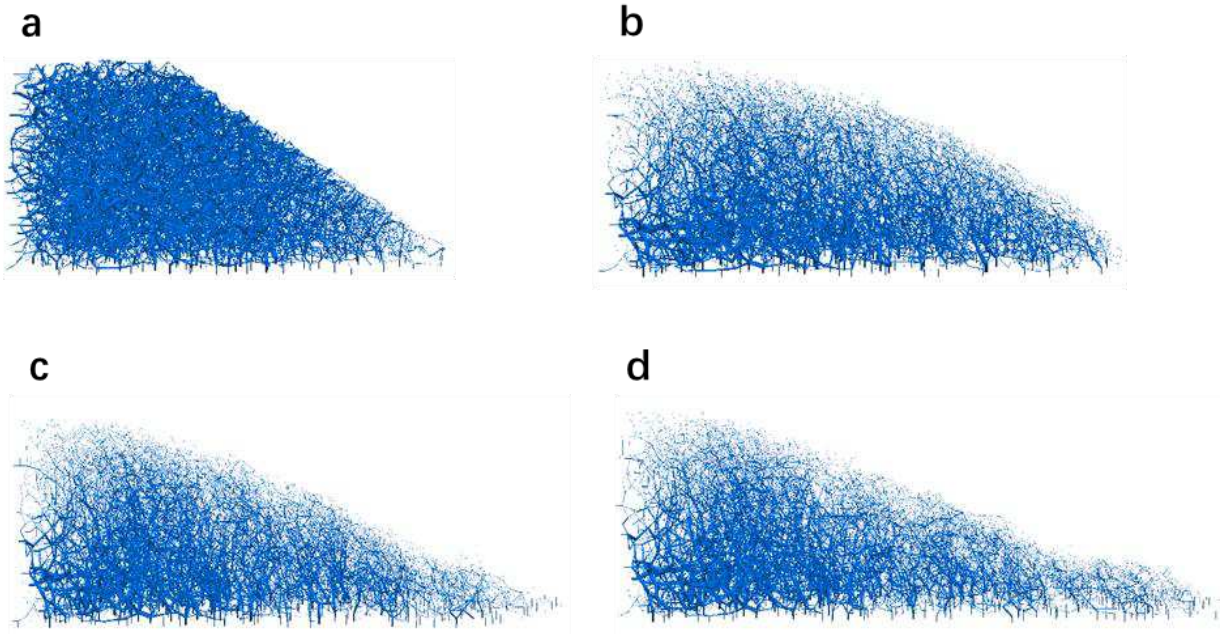

Figure 6. Evolution process of soil particle force chain in slope under rainfall. (**a**) The force chain of slope soil particles in initial state;(**b**) The force chain of soil particles in slope when the model calculated 20000 steps; (**c**) The force chain of soil particles in slope when the model calculated 60000 steps; (**d**) The force chain of soil particles in slope when the model calculated 100000 steps.

Calculation results of coordination number of slope soil particles. Figure 7 shows the cloud atlas of changes in the coordination number of slope soil particles during rainfall. The coordination number of soil particles on the slope gradually decreased due to the continuous effect of rainfall. In such circumstances, the coordination number of soil particles on the upper slope and on the slope surface of the saturated zone significantly reduced, and it slightly reduced in the unsaturated zone inside the slope. This indicates weak contact and poor structural stability between particles in the rain-affected areas, but fair contact and favourable stability between particles in the unsaturated zone. As shown in Figs. 7 (c) and (d), at the time step of 60,000, the coordination number in the saturated zone, especially that at the top of the slope, decreased, while that inside and at the bottom of the slope increased. These observations imply that poor contact between the particles in the upper slope, the gradual downward movement of the particles and their accumulation at the foot of the slope led to the compactness and

good stability of the lower slope under the influence of the fluid.

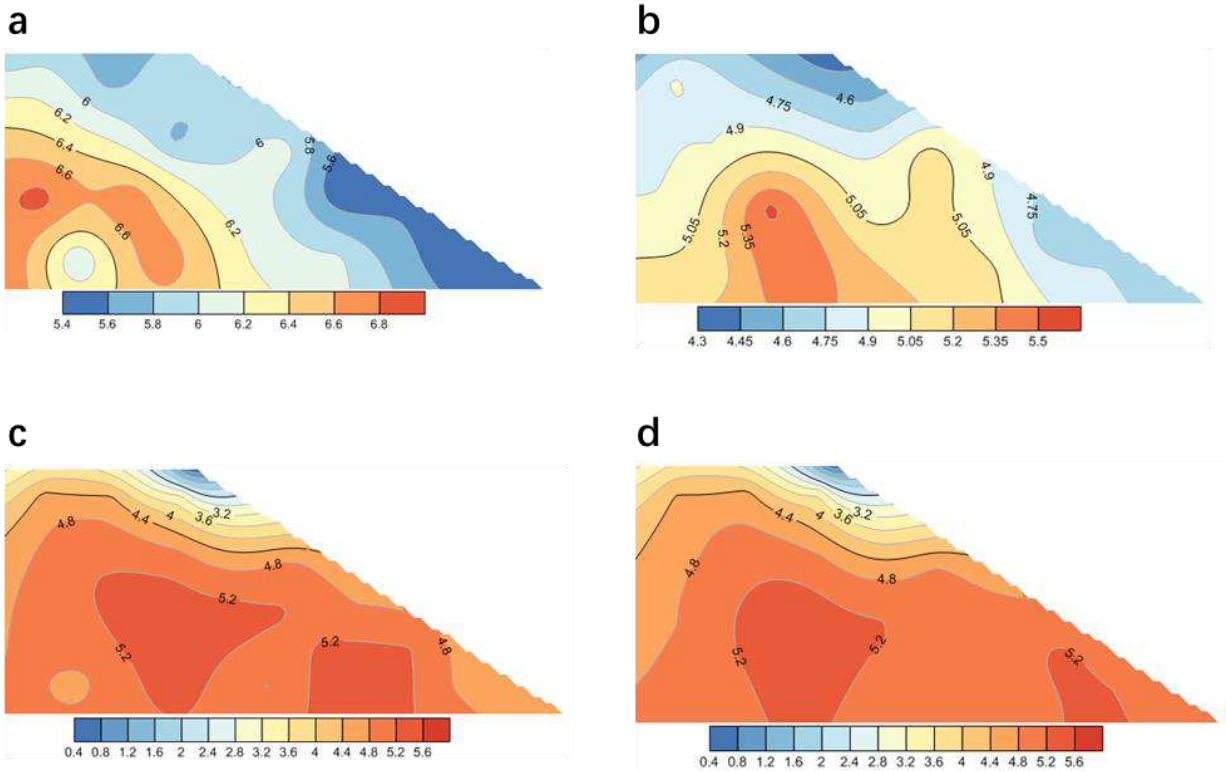

Figure 7. The change process of soil particle coordination number in slope under rainfall. (**a)** Distribution of particle coordination number of slope soil at initial time; (**b)** Distribution of soil particle coordination number in slope when the model calculated 20000 steps; (**c)** Distribution of soil particle coordination number in slope when the model calculated 60000 steps; (**d)** Distribution of soil particle coordination number in slope when the model calculated 100000 steps.

Discussion.

Coal-bearing soil slopes are easily weathered, softened, and disintegrated by water; hence, treating them as discontinuous media for DEM calculations and analyses is reasonable. Comparison of the calculation results simulated by DEM with the results of the outdoor rainfall test concluded the following. Both the methods showed that rainfall-induced erosion was a crucial factor in the failure of coal-bearing soil slopes. Moreover, the slope slip surface was an approximately linear segment. Finally, the erosion range of the model slope was very close to the status of the slip surface calculated and predicted by CFD–DEM coupling. In this study, the rationality of the CFD–DEM fluid–solid coupling method for simulating the rainfall-induced failure of coal-bearing soil slopes was demonstrated. In addition, the feasibility of simulating and analysing the Newton's law of motion of discrete media in geotechnical engineering was verified using the CFD–DEM fluid–solid coupling model[30].

As an important indicator, macroscopic mechanical properties reflect particle movement, thickness, position and density of the force chain, and they provide an intuitive representation of particle forces and movement changes. During rainfall, the force chain significantly stretched along the slope, the slope became gentle and the force chains at the top and on the slope surface decreased and became sparse, implying instability and massive movement of the particles in the saturated zone. Under the combined action of fluid and particles in the upper slope, the force chain in the lower slope became dense and thick, showing enormous contact forces between particles in the slope and the stability of the zone concerned. Through the simulated slope rainfall test, the analysis of force chain changes revealed the failure evolution process of the slope under the influence of

rainfall, which allowed us to deeply understand the failure mechanism of coal-bearing soil slopes.

From the above, simulating and analysing the stability of slopes in discrete media was possible via the introduction of the CFD–DEM fluid–solid coupling model. In addition to serving as a theoretical basis for the protection design and construction of the coal-bearing soil slope in the study area, the research results are expected to encourage the effective analysis of macroscopic mechanical laws in discrete media from a micro–macro perspective in geotechnical engineering.

Conclusion

(1) In an outdoor rainfall test, erosion ditches were formed at different depths on the slope surface by rainwater washing, which is the main failure mode of slope soil. The maximum depth of the ditches was 0.36 m, which was in the mid-upper slope. The failure modes of coal-bearing soil slope simulated by CFD–DEM fluid–solid coupling were consistent with the results of outdoor rainfall test. The prediction of the slope slip surface was an approximately linear segment. The feasibility of using CFD–DEM fluid–solid coupling model in the stability analysis of coal-bearing soil slopes was validated by considering the similarity to the actual model slope in the range of rainwater erosion.

(2) During rainfall, microscopic parameters, such as the force chain, coordination number and porosity of the slope soil particles, changed and were directly related to the macroscopic mechanics of slope soil. Therefore, by analysing the changes in the microparameters of particles, we were able to understand the failure evolution rules of coal-bearing soil slopes under the influence of rainwater and to analyse the failure mechanism of coal-bearing soil slopes with discontinuous media from the micro–macro perspective.

(3) The results of this paper show that it is feasible to simulate the stability of discrete medium slope by combining discrete element method and computational fluid dynamics method. The research results not only provide theoretical basis for the protection design and construction of coal-bearing soil slope in this area, but also provide a new way to better analyze the macro mechanical laws of discrete medium geotechnical engineering from the micro perspective.

Data Availability

The data used to support the findings of this study are available from the corresponding author upon request.

References

1. Lewis, R.W. & Schrefler, B. A. The finite element method in the deformation and consolidation of porous media. *John Wiley & Sons Inc.* New York, NY, 3. (1987).
2. Zienkiewicz, A. H. C. & Chan, M. Computational geomechanics with special reference to earthquake engineering. *International Journal for Numerical & Analytical Methods in Geomechanics* **25**,107-107. (2015).
3. Trussell, R. R. & Chang, M. Review of flow through porous media as applied to head loss in water filters. *Journal of Environmental Engineering* **125**, 998-1006. (1999).
4. Mazari, M. & Arulanandan, K. Numerical prediction for model no 1,Verification of numerical procedures foe the analysis of soil liquefaction problems. Proceedings of the International Conference on the Verification of numerical procedures for the analysis of soil liquefaction problems. 179-785 (Davis, California, 1993).
5. Tsuji, Y., Kawaguchi, T. & Tanaka, T. Discrete particle simulation of two-dimensional fluidized bed. *Powder Technology* **77**, 79-87. (1993).
6. Xu, B. H. & Yu, A. B. Numerical simulation of the gas-solid flow in a fluidized bed by combining discrete particle method with computational fluid dynamics. *Chemical Engineering Science* **52**, 2785-2809. (1997).

7. Xu, B. H., Yu, A. B., Chew, S. J. & Zulli, P. Numerical simulation of the gas-solid flow in a bed with lateral gas blasting. *powder technology* **109**, 13-26. (2000).
8. Yu, A. & Xu, B. Particle-scale modelling of gas-solid flow in fluidization. *Journal of Chemical Technology & Biotechnology* **78**, 111-121. (2003).
9. Chu, K. W. & Yu, A. B. Numerical simulation of complex particle–fluid flows. *Powder Technology* **179**,104-114. (2008).
10. Chu, K. W., Wang, B., Xu, D. L., Chen, Y. X. & Yu, A. B. CFD-DEM simulation of the gas-solid flow in a cyclone separator. *Chemical Engineering Science* **66** , 834-847. (2011).
11. Zhou, Z. Y., Kuang, S.B., Chu, K. W. & Yu, A. B. Discrete particle simulation of particle–fluid flow: model formulations and their applicability. *Journal of Fluid Mechanics* **661**, 482-510. (2010).
12. Guo, Y., Kafui, K. D., Wu, C.Y., Thornton, C. & Seville, J. P. K. A coupled DEM-CFD analysis of the effect of air on powder flow during die filling. *AICHE Journal* **55**, 49-62. (2009).
13. Amritkar, A., Deb, S. & Tafti, D. Efficient parallel CFD-DEM simulations using OpenMP. *Journal of Computational Physics* **256**, 501-519. (2014).
14. Adema, A. T., Yang, Y. & Boom, R. Discrete element method-computational fluid dynamic simulation of the materials flow in an iron-making blast furnace. *ISIJ international* **50**, 954-961. (2010).
15. Nakamura, H., Iwasaki, T. & Watano, S. Numerical simulation of film coating process in a novel rotating fluidized bed. *Chemical & Pharmaceutical Bulletin* **54**, 839-846. (2006).
16. Renzo, A. D. & Maio, F. P. D. Homogeneous and bubbling fluidization regimes in DEM–CFD simulations: Hydrodynamic stability of gas and liquid fluidized beds. *Chemical Engineering Science* **62**, 116-130. (2007).
17. Li, T., Garg, R., Galvin, J. & Pannala, S. Open-source MFIX-DEM software for gas-solids flows: Part II-Validation studies. *Powder Technology* **220**, 138-150. (2012).
18. Chiesa, M., Mathiesen, V., Melheim, J. A. & Britt, H. Numerical simulation of particulate flow by the Eulerian-Lagrangian and the Eulerian–Eulerian approach with application to a fluidized bed. *Computers & Chemical Engineering* **29**, 291-304. (2005).
19. Tsuji, T., Yabumoto, K. & Tanaka, T. Spontaneous structures in three-dimensional bubbling gas-fluidized bed by parallel DEM–CFD coupling simulation. *Powder Technology* **184**, 132-140. (2008).
20. Shamy, U. E. & Zeghal, M. Coupled continuum discrete model for saturated granular soils. *Journal of Engineering Mechanics* **131**, 413-426. (2007).
21. Zhou, J., Zhou, K. M., Yao, Z. X. & Bai, Y. F. Numerical simulation of piping-filter prevention in sandy soil by discrete element method. *Journal of Hydraulic Engineering* **39**, 17-24. (2010).
22. Lou, Y., Gong, X. N. & Wu, R. Q. Analysis and simulation of fluid-particles interaction with particle flow code. *Journal of Zhejiang University(Engineering Science)* **41**, 1932-1936. (2007).
23. Liu, Y., Zhou, J. & Fu, J. X. Fluid-particle coupled model for saturated sand and its application to liquefaction analysis. *Journal of Hydraulic Engineering* **40**, 250-256. (2009).
24. Zhao, J. & Shan, T. Coupled CFD-DEM simulation of fluid–particle interaction in geomechanics. *Powder Technology* **239**, 248-258. (2013).
25. Jiang, M. J. & Zhang, W. C. Coupled CFD-DEM method for soils incorporating equation of state for liquid. *Chinese Journal of Geotechnical Engineering* **36**, 793-801. (2014).
26. Khalili, Y. & Mahboubi, A. Discrete simulation and micromechanical analysis of two-dimensional saturated granular media. *Particuology* **15**, 138-150. (2014).
27. Wang, Y., Ai, J. & Yang, Q. A CFD-DEM coupled method incorporating soil inter-particle rolling resistance. *Rock and Soil Mechanics* **38**, 1771-1780. (2017).
28. Issa, R. I. Solution of the implicitly discretised fluid flow equations by operator-splitting. *Journal of Computational Physics* **62**, 40-65. (1986).

29. Shi, C., Zhang, Q. & Wang, S. N. Particle flow (pfc5.0) numerical simulation technology and its application. *Rock and Soil Mechanics* **39**, 36-37. (2018).
30. Li, X. & Zhao, J. Numerical simulation of dam break by a coupled CFD-DEM approach. *Japanese Geotechnical Society Special Publication* **2**, 691-696. (2016).

Acknowledgements

The work was supported by the National Natural Science Foundation of China (Grant No. 52068053) and the Superiority Science and Technology Innovation Team Project of Nanchang City (Grant No. 2017CXTD012).

Author contributions

Z. H. designed the study. Z.H. and Z.B. carried out the construction of CFD-DEM numerical model and the calculation of the program. F.H.R. and W.C. analyzed the data and drew some figures. C.K. carried out the data collection and analysis of outdoor test. Z.H. wrote the main manuscript. All authors reviewed and approved the final manuscript.

Competing interests

The authors declare no competing interests.

Figures

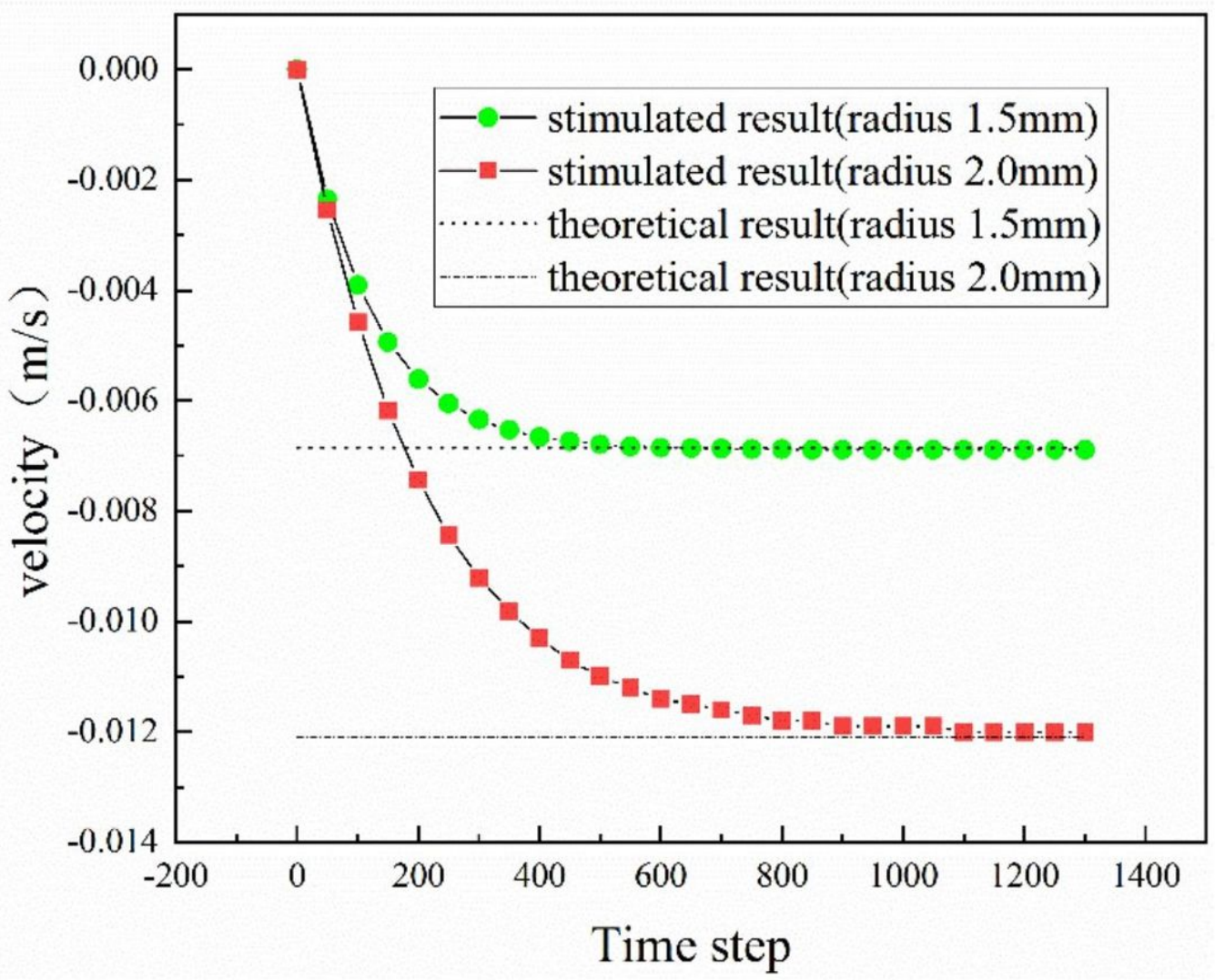

Figure 1

Velocity of falling particles.

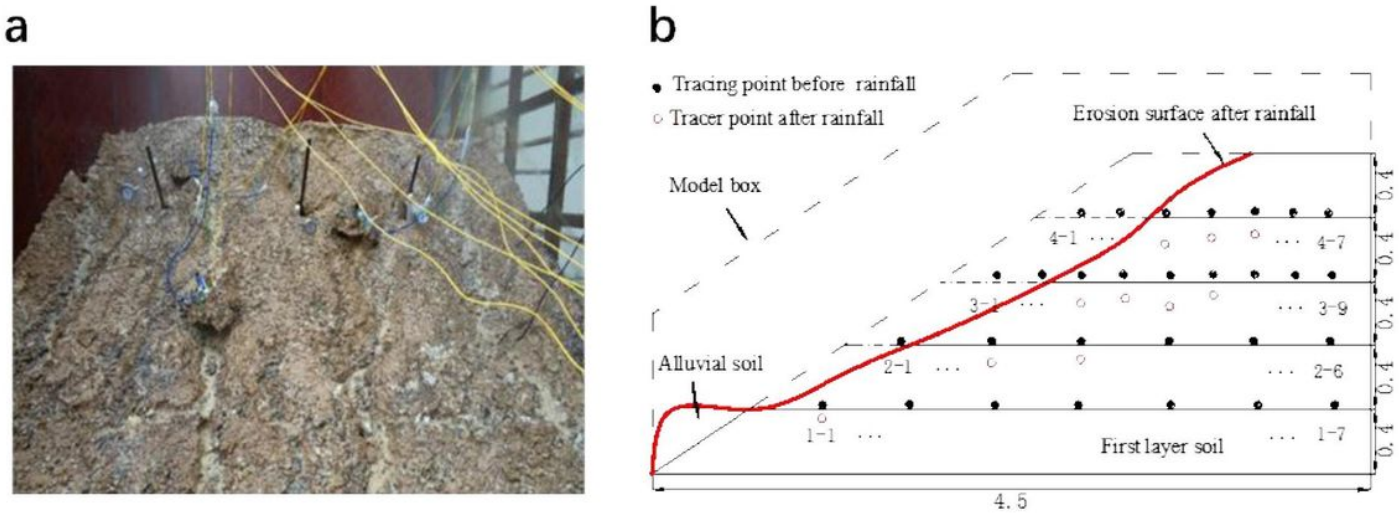

Figure 2

The site of slope failure test. (a) Front of slope model; (b) Schematic diagram of soil movement of tracer point on the site of slope failure test. (unit: m)

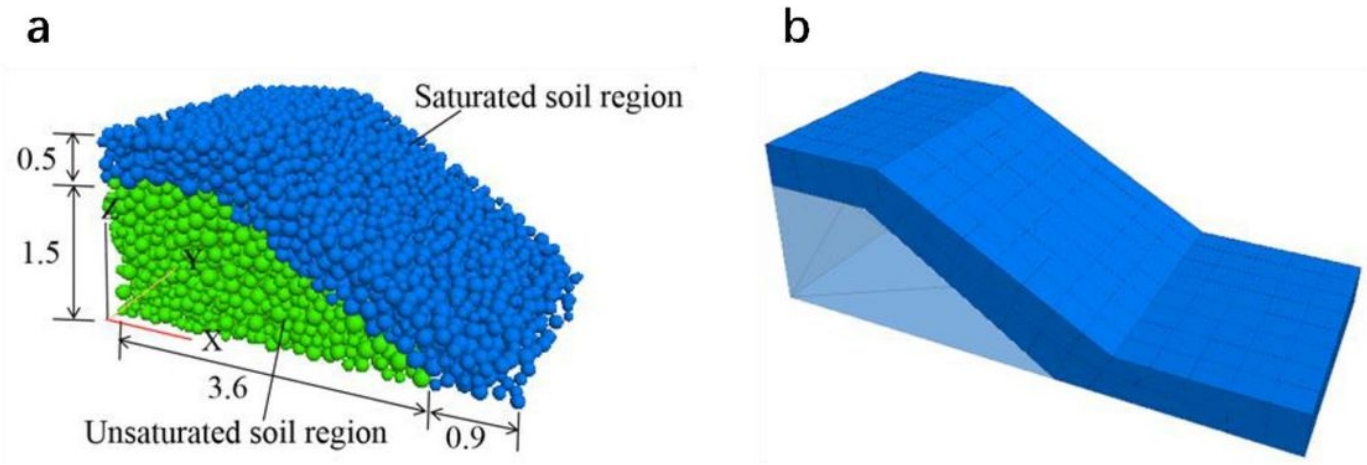

Figure 3

The fluid-solid coupling（CFD-DEM） calculation model of slope under rainfall infiltration. (a) The soil in the rainwater infiltration area is stratified;(b) Set up the seepage grid. (unit: m)

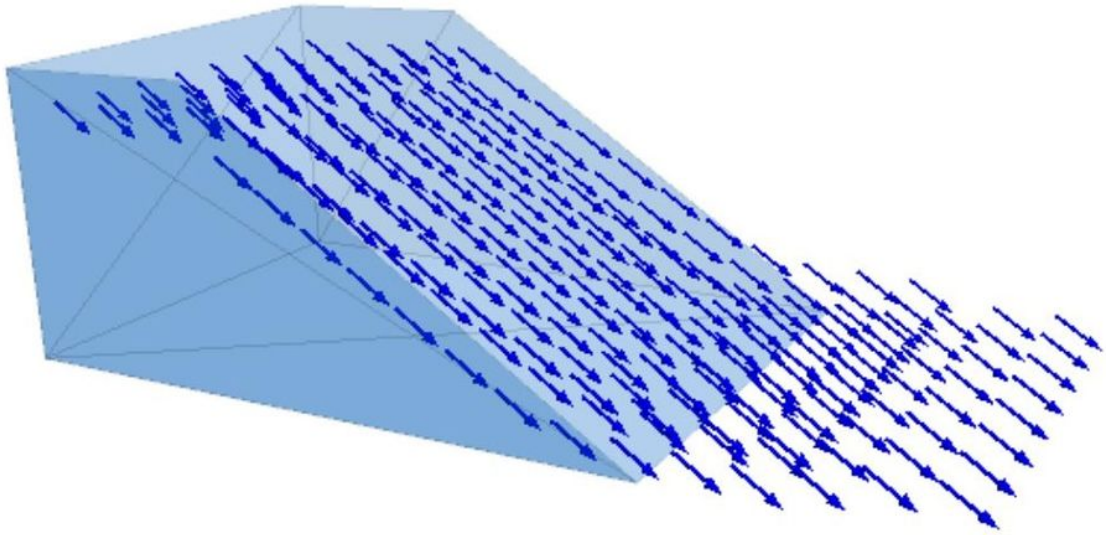

Figure 4

Direction of fluid movement in slope saturated area.

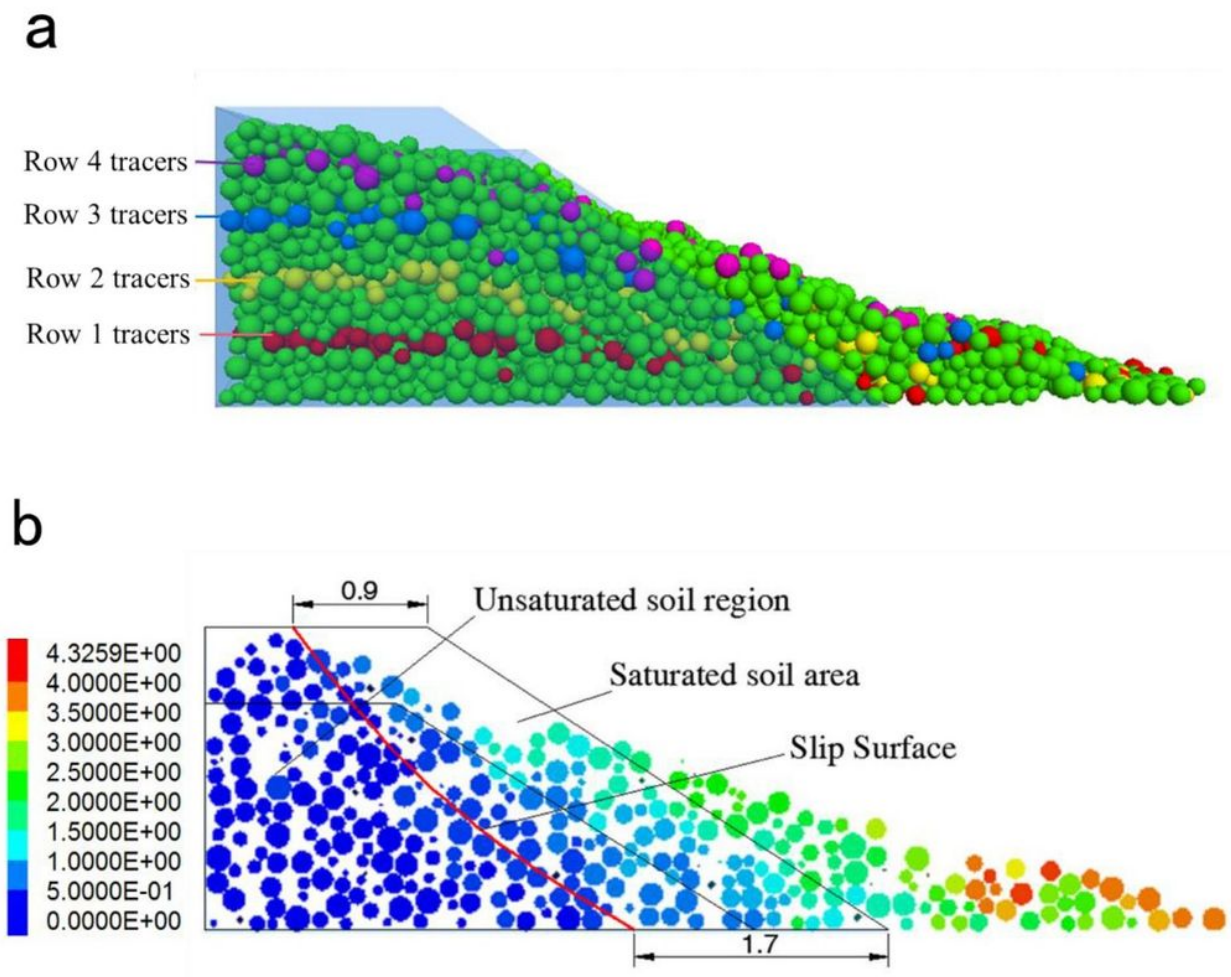

Figure 5

Schematic diagram of the overall particle movement of the slope. (a) Overall particle displacement diagram of slope;(b) Schematic diagram of slope sliding surface. (unit: m)

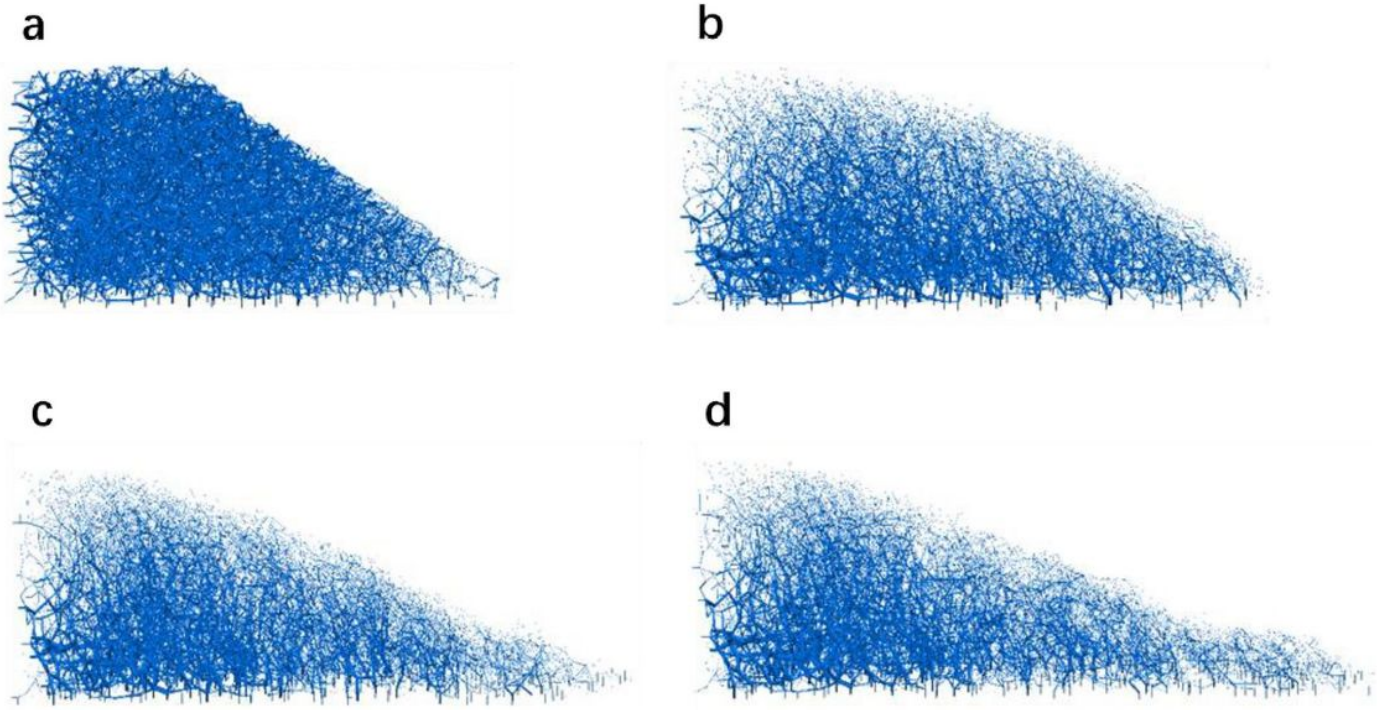

Figure 6

Evolution process of soil particle force chain in slope under rainfall. (a) The force chain of slope soil particles in initial state;(b) The force chain of soil particles in slope when the model calculated 20000 steps; (c) The force chain of soil particles in slope when the model calculated 60000 steps; (d) The force chain of soil particles in slope when the model calculated 100000 steps.

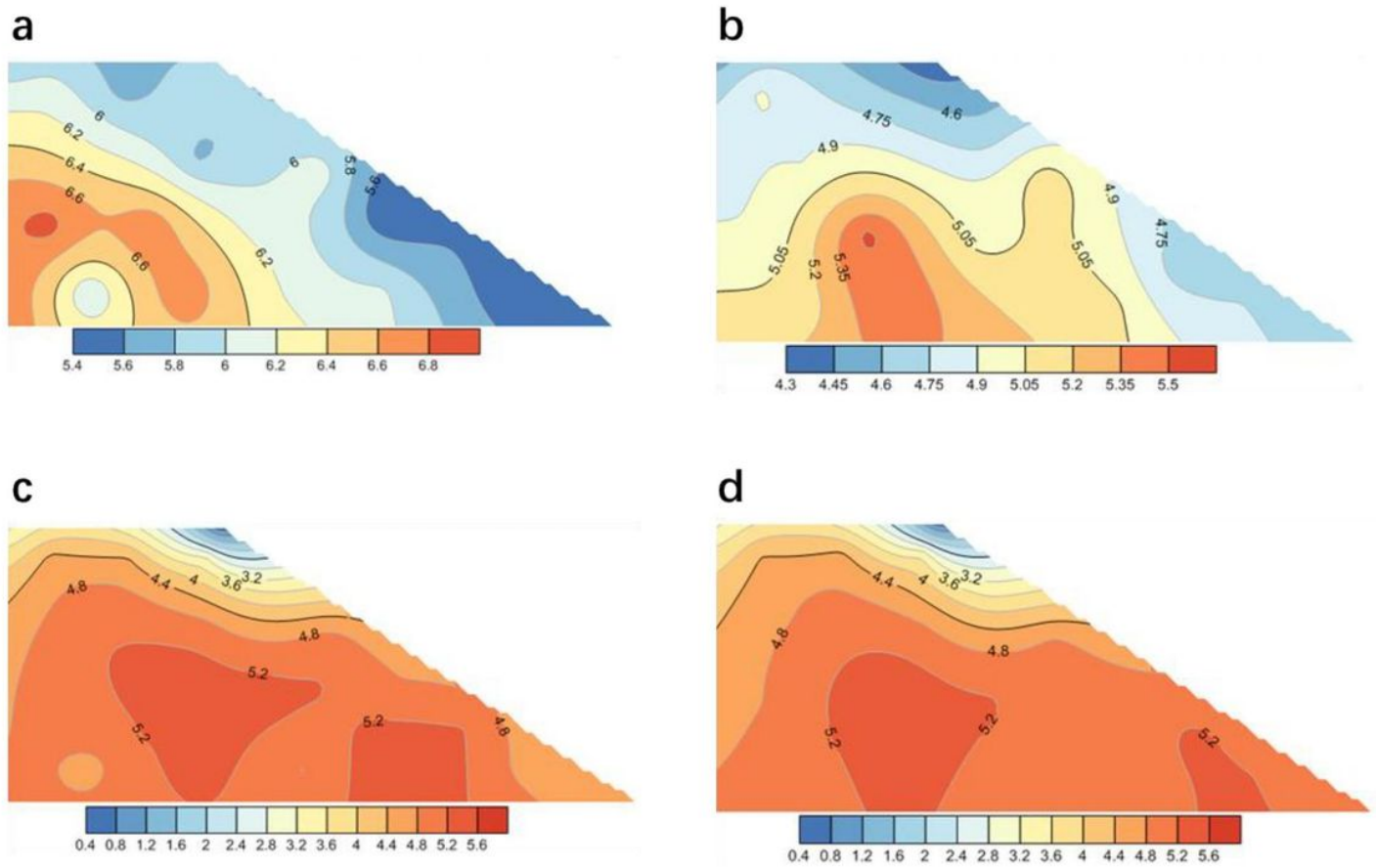

Figure 7

The change process of soil particle coordination number in slope under rainfall. (a) Distribution of particle coordination number of slope soil at initial time; (b) Distribution of soil particle coordination number in slope when the model calculated 20000 steps; (c) Distribution of soil particle coordination number in slope when the model calculated 60000 steps; (d) Distribution of soil particle coordination number in slope when the model calculated 100000 steps.